JOURNAL OF SPACECRAFT AND ROCKETS
Vol. 40, No. 5, September–October 2003

Approach for Combining Spacecraft Attitude and Thermal Control Systems

Renuganth Varatharajoo,* Ralph Kahle,† and Stefanos Fasoulas‡
Dresden University of Technology, 01062 Dresden, Germany

Coupling of existing spacecraft subsystems could be an alternative to reduce the emerging cost, decrease the system volume/mass and complexity, increase the reliability, and enhance the overall performance of future spacecraft. Therefore, a new concept to combine the attitude and thermal control systems is presented. The concept is based on electric conducting fluids used in a closed loop for the attitude and thermal control systems. The potential coupling is discussed for two alternative setups incorporating electromagnetic pumping and thermoelectric phenomena, respectively. The corresponding equations are derived and the end-to-end system demonstration is performed. The results demonstrate that the new concept could replace the existing subsystems using current available technology, especially the thermoelectric option, when used as a combined attitude actuator and thermal radiator.

Nomenclature

A	=	cross section, m^2
B	=	magnetic flux density, T
b	=	duct width, mm
c_p	=	specific heat of gallium at 303 K, equal to $372\ J \cdot kg^{-1}K^{-1}$
D	=	hydraulic diameter, $2hb/(h+b)$, m
f	=	friction coefficient
Ha	=	Hartmann number, $\sqrt{(\sigma_{ec}/\rho\nu)}Bh$
h	=	duct height, mm
I	=	current, A
J_f, J_{sat}	=	fluid and satellite moments of inertia, $kg \cdot m^2$
j	=	current density, A/m^2
K_i	=	integral attitude control gain, N · m/s
K_P	=	proportional attitude control gain, N · m/rad
L	=	angular momentum, N · ms
l	=	length, m
m	=	mass, kg
n	=	number of magnetohydrodynamics pumps
p_{inlet}, p_{outlet}	=	inlet and outlet duct pressures, N/m^2
q	=	heat flow, W
R	=	duct radius, m
Re	=	Reynolds number, VD/ν
T_D	=	external disturbance torques, N · m
T_S	=	exerted torque on the satellite body, N · m
t	=	time, s or min
V	=	fluid velocity, m/s
v	=	proportional attitude torque command, T_{cmd}, N · m
Δp_{loss}	=	pressure drop due to the duct friction, N/m^2
ε	=	onboard errors
θ_{ref}, θ_{sat}	=	reference and true satellite attitudes, rad or deg
κ	=	thermal diffusivity, $\lambda/\rho c_p$, m^2/s
λ	=	thermal conductivity of gallium at 303 K, equal to $40.6\ W \cdot m^{-1}K^{-1}$
ν	=	kinematic viscosity of gallium at 303 K, equal to $3.49 \times 10^{-7}\ m^2s^{-1}$
ρ	=	density of gallium at 303 K, equal to $5907\ kg \cdot m^{-3}$
σ_{ec}	=	electrical conductivity of gallium at 303 K, equal to $3.7 \times 10^6\ \Omega^{-1}m^{-1}$
τ	=	time constant, s
Ω_f	=	fluid angular velocity, rad/s
Ω_o	=	orbital frequency, rad/s

Received 17 July 2002; revision received 8 February 2003; accepted for publication 8 March 2003.

*Research Staff, Institute for Aerospace Engineering; on leave from Research Staff, Department of Aerospace Engineering, University Putra Malaysia, 43400 Serdang, Selangor, Malaysia; renu99@gmx.de.

†Research Assistant, Institute for Aerospace Engineering.

‡Professor for Space Systems and Utilizations, Institute for Aerospace Engineering. Member AIAA.

Introduction

SPACECRAFT usually experience temperature gradients in their structures because of sun illumination conditions and because of the heat generated by different electrical energy consuming subsystems. To keep the maximum temperature on spacecraft below a certain level, and to avoid thermal stresses, the excess generated heat is usually dissipated by radiation. Radiators, for example, heat pipes, with relatively high surface areas are normally used to handle this task.

In this paper, the basic idea is to couple the thermal control system with the attitude control system by utilizing an electrical conductive fluid that circulates in a closed loop to simultaneously serve as heat conductor and momentum generator. The fluid circulation could be influenced by a variation of external and internal effects, for example, electric and magnetic fields and temperature gradients. Thus, the conventional heat pipes could be replaced by a duct system in which the fluid with a reasonable heat transfer coefficient circulates. The fluid should also have good electrical conductivity to minimize the driving power requirement for an unidirectional motion using the electric fields. As a result, an angular momentum can be generated along the fluid circulation axis. The generated angular momentum could then contribute to the spacecraft attitude control. Additionally, this fluid motion would not depend on the natural convection phenomena, and the heat transport or heat dissipation process could be enhanced. The fluid chosen here as an example for the discussion is liquid–metal gallium. Gallium's melting point is at 303 K, and if desired, this value can be dropped by adding indium (24%) and tin (16%) compounds. Nevertheless, other electric conducting fluids with lower melting temperatures could also be considered. However, these temperatures should be in the order of the operating temperature of spacecraft. Such a combined attitude and thermal control system is described in Refs. 1–3. However, the existing literature does not emphasize on the mathematical models for a comprehensive end-to-end system demonstration. Therefore, the present study deals with an initial development of useful models that allow a

systematic investigation and demonstration of the system. The system is proposed for medium-class satellites, for example, 100–500 kg, in this study.

Two concepts are introduced based on magnetohydrodynamics (MHD) for the investigation that follows. The first concept assumes a simple electromagnetic pumping of the fluid, and the second concept benefits from the thermoelectric effect. For the electromagnetic pump driven combined attitude and thermal control system (CATCS), permanent magnets and electrodes are used to drive the gallium flow. The flow can be influenced by varying the current through the electrodes. The second concept makes use of an existing temperature gradient in satellites to create a flow through coupling of thermoelectric and magnetic fields (thermoelectric-driven CATCS). In this system, the electrical current is generated by the temperature gradient between metal pairs, for example, cobalt and liquid–metal gallium. Hence, when a magnetic field is introduced near the generated electric field, a fluid flow is induced. Therefore, the onboard electrical power is not fully needed for this option to drive the fluid, which makes the system much more attractive. Simultaneously, this option could wield the heat transport from particular heat spots on satellites, for example, equipment, sun-exposed walls, etc. The basic system configurations, their mathematical formulations, and the most important results are presented.

Electromagnetic-Pump-Driven CATCS

The configuration for the electromagnetic-pump-driven CATCS is shown in Fig. 1a. The liquid–metal gallium flows in a duct with rectangular cross section (Fig. 1b). The fluid contacts the satellite's walls, so that the excess heat is transported, and consequently, a cooling process occurs. Because of the flow velocity, an angular momentum is generated, which can be used for attitude control purposes. This system consists of permanent magnets and electrodes. The flow velocity of gallium can be influenced by varying the current and/or magnetic flux density. However, for increasing the flow velocity, it seems more convenient to introduce a higher current than a higher magnetic flux (cumbersome for the magnet compartment).

The principal parameter for the evaluation is the generated flow velocity, from which other characteristic system data can be derived, for example, angular momentum and heat transport capability.

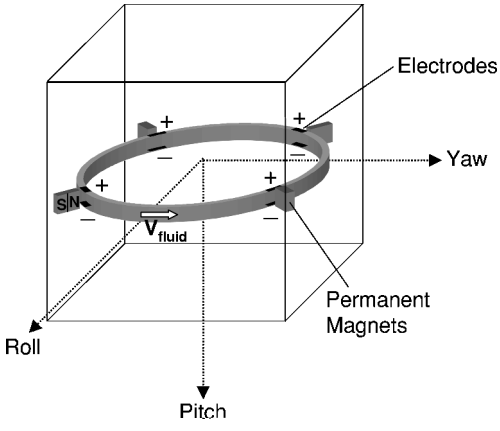

a)

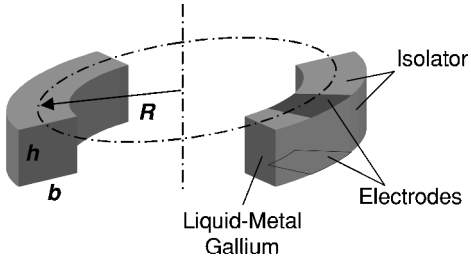

b)

Fig. 1 Electromagnetic-pumps driven CATCS.

For the fluid velocity estimation, it is assumed that the vectors of the magnetic flux density and current applied over the duct height are perpendicular and have only one nonzero component. Thus, a Lorentz force F_L will be induced normal to the cross section of the fluid flow direction (resulting motion):

$$F_L = hIB \tag{1}$$

When it is assumed that this force is constant over the cross section $A = hb$ (Fig. 1b), the equivalent pumping pressure is

$$\Delta p_{\text{pump}} = F_L/A = IB/b \tag{2}$$

Then, the fluid velocity can be estimated by using Bernoulli's equation:

$$p_{\text{inlet}} = p_{\text{outlet}} + \Delta p_{\text{loss}} - n\,\Delta p_{\text{pump}} \tag{3}$$

For a closed system, inlet and outlet pressures are equal. Thus, Eq. (3) reduces to

$$\Delta p_{\text{loss}} = n\Delta p_{\text{pump}} \tag{4}$$

The pressure drop due to the duct friction[4] can be estimated from

$$\Delta p_{\text{loss}} = f(l/D)(\rho/2)V^2 \tag{5}$$

The critical Reynolds number (see Ref. 5) for a laminar flow in pipe loops is

$$Re_{\text{crit}} = 16.5\sqrt{R/D}, \qquad R/D \geq 0.001 \tag{6}$$

If it is assumed that $R = 0.5$ m and $D \approx 0.01$ m in Fig. 1, the critical Reynolds number would be $Re_{\text{cri}} \approx 120$. If a low velocity of about 0.01 m/s is assumed for this reference configuration, the Reynolds number will be about 286. Therefore, the friction coefficient for the turbulent case has to be considered. For hydraulically smooth walls with rectangular cross section and $Re < 10^4$, this coefficient[6] is approximately

$$f \approx 0.32/Re^{0.25} \tag{7}$$

Inserting these equations in Eq. (4) yields, for the flow velocity,

$$V = \left(\frac{nIBD^{1.25}}{0.32b\nu^{0.25}\pi R\rho}\right)^{\frac{4}{7}} \tag{8}$$

It is obvious from Eq. (8) that the maximum velocity is restricted by the available magnetic flux density, current, and mass of the system [R, $D(b, h)$, ρ].

The estimated mass of the housing, permanent magnets and power supply are approximately 25% of the overall system mass. In fact, the system's mass is mainly composed of the fluid mass. Therefore these parameters are used to estimate the fluid inertia and the generated angular momentum along the fluid circulation axis. Figures 2 and 3 show the fluid velocity and angular momentum calculated as a function of applied current. In Fig. 2 the magnetic flux density is fixed to $B = 0.3$ T and four pumps are used for the calculation; only the duct cross section (height and width) and radius are varied. Three design options are analyzed: a) $R = 0.15$ m, $h = 30$ mm, $b = 10$ mm, $m = 1.67$ kg, $J_f \approx 0.04$ kg·m^2, and $Re_{\text{cri}} = 52$; b) $R = 0.3$ m, $h = 30$ mm, $b = 5$ mm, $m = 1.67$ kg, $J_f \approx 0.15$ kg·m^2, and $Re_{\text{cri}} = 95$; and c) $R = 0.5$ m, $h = 20$ mm, $b = 5$ mm, $m = 1.86$ kg, $J_f \approx 0.46$ kg·m^2, and $Re_{\text{cri}} = 130$. The highest angular momentum obtained is about 0.08 N·ms. Because of the deficiency in generated momentums, the magnetic flux density is increased to achieve higher fluid velocities and eventually higher momentums. The results shown in Fig. 3 show the influence of magnetic flux density for fixed system dimensions: $n = 4$, $R = 0.5$ m, $h = 20$ mm, $b = 5$ mm, $m = 1.86$ kg, $J_f \approx 0.46$ kg·m^2, and $Re_{\text{cri}} = 130$. The maximum angular momentum obtained for this configuration is about 0.11 N·ms.

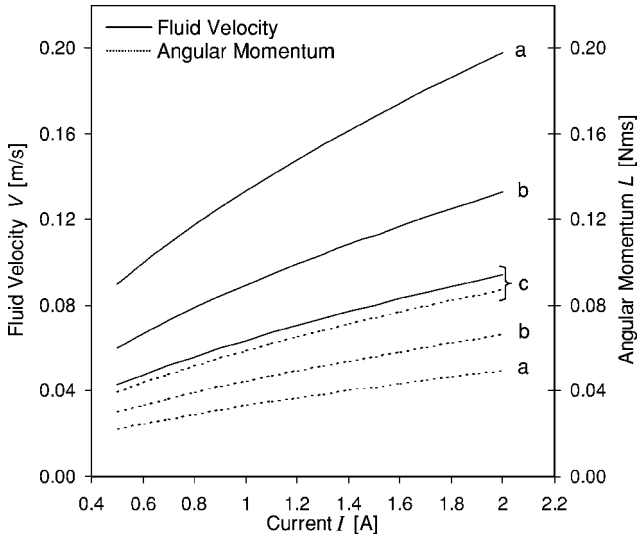

Fig. 2 Fluid velocity and angular momentum as a function of current.

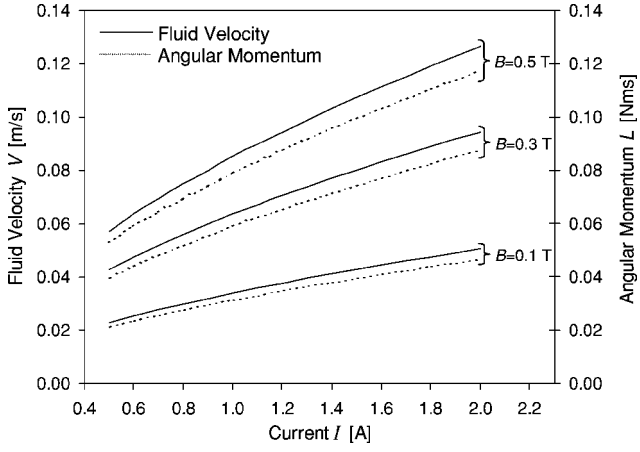

Fig. 3 Fluid velocity and angular momentum as a function of current; *B* is varied.

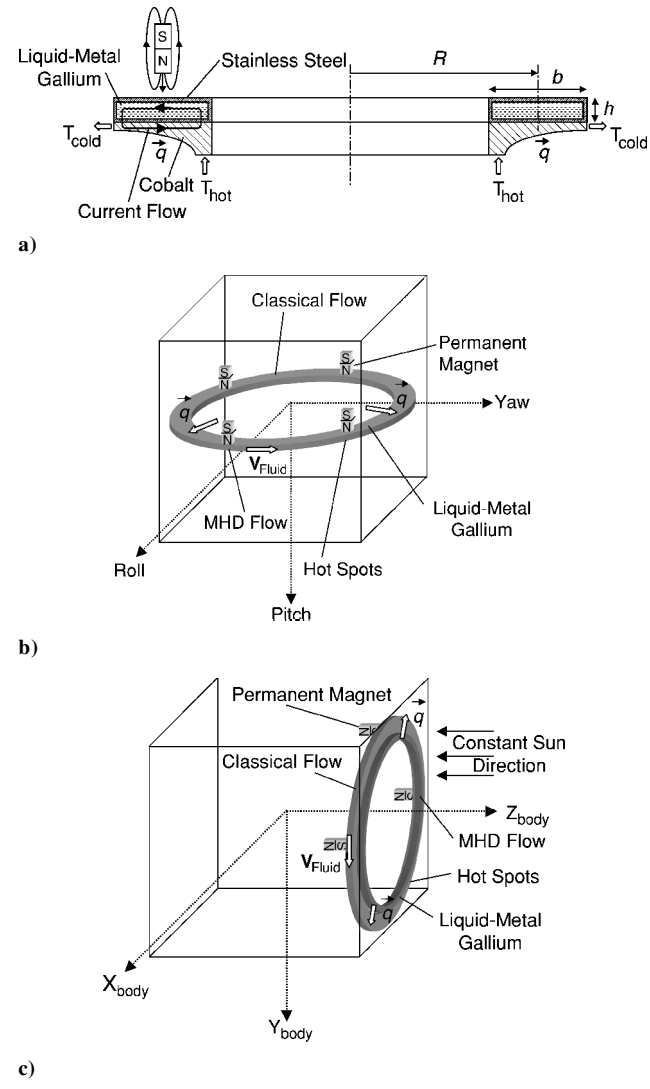

Fig. 4 Thermoelectric-driven CATCS.

Another important parameter to be estimated is the system power consumption. The voltage drop U_e in electromagnetic pumps is caused by the electrical resistance of liquid metal R_e together with the current, for example, 1–2 A, and the hydrodynamic electrical transfer C_{he} and can be calculated[7] according to

$$U_e = C_{\text{he}} AV + R_e I = BhV + (h/bl_e\sigma_{\text{ec}})I \tag{9}$$

where l_e is the length of electrodes ($\approx$0.01 m) and $C_{\text{he}} = B/b$. For this configuration, the total power consumption is not higher than 0.1 W, which is much lower compared to that of typical momentum wheels,[8] for example, 4–15 W, for medium-class satellites. The low-power consumption for the complete system is remarkable, but its achievable angular momentums are lower ($\approx$0.1 N · ms) compared to the momentum wheels.

It is evident that higher momentums could be achieved by increasing the current, increasing magnetic flux density, or placing the fluid farther from the circulation axis. However, the constraints are the available bus current, mass, and dimension of the satellite. Therefore, a thermoelectric-driven CATCS, which is expected to generate higher angular momentums, is investigated in the next section.

Thermoelectric-Pump-Driven CATCS

Because the electromagnetic pump system is restricted by the available onboard current, a thermoelectric-pump-driven system, which uses the Seebeck phenomena (see Ref. 9) to achieve a higher current flow, is discussed in the following. A possible system design is shown in Fig. 4a. Here a temperature gradient exists along the thermoelectric generator, for example, cobalt, housing, for example, stainless steel, and fluid, for example, gallium. The difference in thermoelectric power of these conductors will result into an electric current. When magnetic fields are applied to these current flows, the resulting Lorentz forces would induce a fluid motion.

There are different possibilities for implementing such a system on satellites. Figure 4b shows a system that is used to dissipate the excess heat from hot spots to the satellite walls. Such a system could be mounted on any satellite axis. On the other hand, an existing heat source on a satellite side wall due to sun lighting could be redirected to the kernel of the system by employing heat sinks, which would cool down the exposed wall as well. Another possible system is shown in Fig. 4c. The heat from the sun side, for example, for sun observation satellites, is dissipated to the satellite's neighboring walls. In both options, the fluid motion is influenced by adjusting the magnetic flux density acting on the system.

For the thermoelectric-pump-driven CATCS, the performance equations are similar to the equations derived for the electromagnetic pump system. Additionally, only the generated current (thermoelectricity) needs to be estimated in this section. The generated current depends on the thermoelectric power ΔS, temperature gradient ΔT, and electrical conductivity σ_{ec} of the system. Applying Ohm's law, the local current generated in the MHD compartment would be

$$I_{\text{local}} = \sigma_{\text{ec}}(A_e/b)\Delta S\Delta T \tag{10}$$

where the cross section A_e is the mean circumference of duct l_f times duct height h. The MHD compartments account only for about

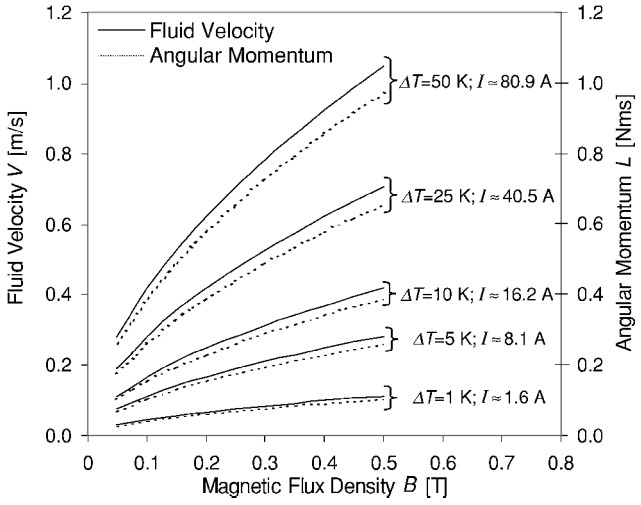

Fig. 5 Fluid velocity and angular momentum as a function of magnetic flux density.

5% of the entire system circumference; thus, each compartment is $l_f \approx 0.05$ m for the reference configuration. On the other hand, the thermoelectric power ΔS is the sum of absolute thermoelectric powers: Stainless steel and gallium have no thermoelectric power, and cobalt has -35 μV/K of thermoelectric power. Subsequently, Eq. (10) can be solved, and Eq. (8) can be evaluated for the fluid velocities.

Figure 5 presents the fluid velocities and the corresponding angular momentums calculated for this option: $n = 4$, $R = 0.5$ m, $h = 5$ mm, $b = 20$ mm, $m = 1.86$ kg, $J_f \approx 0.46$ kg$\cdot$m^2, and $Re_{\text{cri}} = 130$. For a temperature gradient of 50 K, a current of about 80 A would be generated, resulting into an angular momentum of 0.95 N$\cdot$ms. The generated angular momentum is reasonably higher than that of the electromagnetic-pump-driven CATCS. However, this system is unsuitable to be classified as a fluid momentum wheel because higher angular momentums are usually expected from such devices. Instead, this system is comparable to the reaction wheels found in some satellites, for example, Nimbus and Landsat 1 and 2,[10] or some commercially available reaction wheels.[8] Therefore, for comparison reasons, it is important to determine precisely the response time of CATCS when used as an actuator or a fluid reaction wheel on a spacecraft. To determine the response time, the characterization of the unsteady fluid regime is necessary.

Characterization of Unsteady Fluid Regime

The unsteady fluid regime for CATCS consists of the MHD and classical bounded fluid flows (Figs. 4b and 4c). The MHD compartment (system driver) will be investigated for its response time first, then the classical fluid compartment will be analyzed for the same purpose.

MHD Flow Compartment

The MHD compartment in CATCS is shown in Fig. 6, which couples the current density, magnetic flux density, and fluid velocity vector fields. These vectors are assumed to have only one nonzero component as shown in Fig. 6. Thus, the governing MHD equations with respect to the time are

$$V(R, Y, t) = V_\theta(R, t)\{1 - \exp[-Ha(Y/h)]\} \tag{11}$$

$$j(R, Y, t) = j_{Ha}(R, t)\exp[-Ha(Y/h)] + j(R, t) \tag{12}$$

For Hartmann numbers $Ha \gg 1$ (as herein), the Hartmann flow and MHD Couette flow solutions show that the velocity and current variations are localized in a very thin layer close to the wall, whose thickness is of the order of h/Ha (see Refs. 7 and 11). In this case, the time response of MHD system is dominated by the evolution of the core velocity V_θ. In seeking an analytical solution for the transient response, the Navier–Stokes equation (see Ref. 7) for MHD must

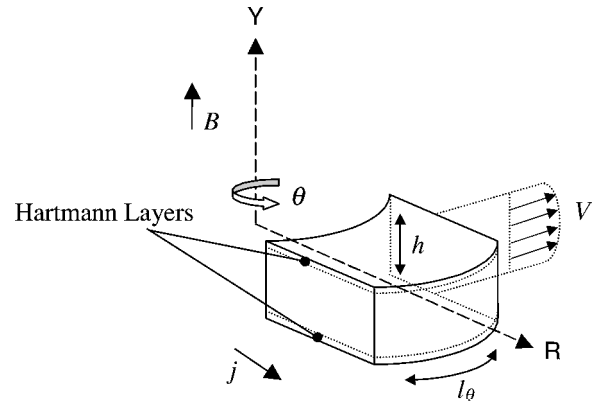

Fig. 6 Two-dimensional MHD fluid compartment.

be employed. When the convection, pressure, viscosity, and gravity terms are neglected, the Navier–Stokes equation reduces for the core flow to

$$\frac{\partial V_\theta}{\partial t}\rho = jB \tag{13}$$

The characteristic of the Hartmann layer for parallel flows is

$$j_{Ha}(R, t) = \sigma_{\text{ec}} B V_\theta(R, t) \tag{14}$$

And, the current density in the core region as a function of Hartmann number and total electric current is

$$j(R, t) = \frac{I}{l_\theta h} - \frac{\sigma_{\text{ec}} B V_\theta(R, t)}{Ha} \tag{15}$$

With these equations, and when $\partial V_\theta/\partial t$ is denoted in Laplace form $sV_\theta(s)$, the core velocity $V_\theta(s)$ between the two Hartmann layers yields

$$V_\theta(s) = \left(I \Big/ 2l_\theta\sqrt{\sigma_{\text{ec}}\rho\nu}\right)\{1/[1 + (h^2/\nu Ha)s]\} \tag{16}$$

The core velocity has an exponential function with a response time τ_{mhd} of $h^2/\nu Ha$. In this investigated example, the estimated time constant is $\tau_{\text{mhd}} = 0.68$ s. Because the Hartmann number is reasonably $Ha \gg 20$ (here $Ha \approx 106$), this time constant would be valid for accelerating and decelerating the system. Such fluid motions can be achieved by varying the magnetic flux density in this investigation.

Classical Flow Compartment

The classical flow dominates about 95% of the fluid flow in CATCS. The pressure of MHD pump accelerating the fluid flow can be expressed as

$$\Delta p_{\text{pump}} = \frac{\partial V}{\partial t}\rho l \tag{17}$$

The final pumping pressure p_{final} must balance the friction pressure drop to achieve the intended fluid velocity V_{final} as in Eq. (4). Therefore, the transient pumping pressure at any instant is

$$\Delta p_{\text{pump}} = p_{\text{final}} - f(l/D)(\rho/2)V_{\text{ins}}^2 \tag{18}$$

or

$$\frac{\partial V}{\partial t}\rho l = p_{\text{final}}\left(1 - \frac{V_{\text{ins}}^2}{V_{\text{final}}^2}\right) \tag{19}$$

where V_{ins} is the mean instantaneous fluid velocity. Hence, the response time τ_{cls} for this classical flow would be

$$\tau_{\text{cls}} = \frac{\rho l V_{\text{final}}^2}{p_{\text{final}}}\int \frac{1}{V_{\text{final}}^2 - V_{\text{ins}}^2}\partial V \tag{20}$$

Apply the boundary conditions $V_{\text{ins}} = 0$ at $t = 0$, and note that the exponential velocity profile attains 99% of V_{final} in a finite time. Equation (20) yields for the response time

$$\tau_{\text{cls}} = 2.646(\rho l V_{\text{final}} / p_{\text{final}}) \tag{21}$$

The corresponding time constant for classical flow in the reference configuration is determined as $\tau_{\text{cls}} = 1.2$ s. As a result, the total response time for CATCS would be $\tau_f = \tau_{\text{mhd}} + \tau_{\text{cls}} = 1.88$ s. With determination of this response time, the attitude control architecture for CATCS (as a fluid reaction wheel) can be investigated.

CATCS Attitude Control Architecture

If the CATCS is intended to be used as an onboard attitude actuator, the selection of drivers is very crucial for the attitude control performance. The drivers should be able to provide the required control torque by adjusting the magnetic flux density acting on the MHD compartments. For the thermoelectric-driven CATCS, neither electromagnets nor combined permanent-electromagnets are suitable as the drivers because of their high-power consumption, for example, 20 and 12 W (four units all together), respectively, for about 1 T of magnetic flux density.[12] Hence, the use of permanent magnets together with linear motors seems favorable. The linear motors are lightweight and have low-power consumption, for example, each is about 28 g and consumes 1.6 W, respectively, for the reference case.[13] Thus, the fluid velocity can be controlled by varying the distance between permanent magnets and fluid housing. As a result, the available duct friction becomes important for fluid braking to have bidirectional control torques $\pm T_S$ on the satellite body. Therefore, the minimum available friction torque at a very low fluid velocity is crucial. For the investigated configuration, the friction torque is approximately 4.5×10^{-4} N · m, corresponding to a low fluid velocity of about 0.01 m/s. This value is much higher than the typical external disturbance torques (e.g. aerodynamics, earth magnetic field, gravity gradient, and solar pressure),[10] which are usually in the order of 10^{-5} N · m for medium-class low-Earth-orbit (LEO) satellites.[14]

The attitude control architecture can now be implemented with the selected driver. The CATCS attitude control architecture is shown in Fig. 7 (thermoelectric option with four MHD pumps, Fig. 4b). Figure 7 presents a proportional–integral (PI)-based attitude control design with an attitude/angle feedback θ_{sat}. Note that the PI attitude controller is chosen as an example for CATCS. In fact, the PI controller shows a good agreement with the attitude stability aspects. On the other hand, although a proportional–integral–derivative controller requires three attitude control gains, it could be also envisaged for CATCS. Generally, an attitude control system can also have a double feedback, that is, the angle θ_{sat}, for example, from star sensor, and the angle rate ω_{sat}, for example, from gyroscope. Therefore, when prefiltering[15] $F(s)$ is introduced in Fig. 7, the numerator term of the system transfer function $H(s)$ is eliminated, and therefore, the transfer function will be identical to that of the architecture with angle and angle rate feedbacks. Note that, as shown in Fig. 7, the displacement d, induced magnetic flux density B, and resulting torque T_f are the physical constants describing the drivers. Their dependencies are given by the linear motor constant k_L, induced flux density constant k_B, and resulting torque constant k_T, respectively. In addition, the system gains are $K_C = 1/n$, and the drivers' constants are equal for an ideal system, that is,

$$k_{L1} = k_{L2} = k_{L3} = k_{L4} = k_L$$

$$k_{B1} = k_{B2} = k_{B3} = k_{B4} = k_B$$

$$k_{T1} = k_{T2} = k_{T3} = k_{T4} = k_T$$

Furthermore, the product of these constants is defined as $k_L \times k_B \times k_T = k_G$. The ε in Fig. 7 represents the torque accuracy of CATCS: $\varepsilon = 1 \pm \varepsilon_T$, where ε_T is the internal torque gain errors. For an ideal system, ε_T would be equal to zero so that $\varepsilon = 1$. Subsequently, the transfer function for satellite's dynamics is

$$\theta_{\text{sat}}/\theta_{\text{ref}} = F(s)H(s) \tag{22}$$

where

$$F(s) = 1/[1 + (K_P/K_i)s] \tag{23}$$

and yields

$$\frac{\theta_{\text{sat}}}{\theta_{\text{ref}}} = 1 \Big/ \left(\frac{J_{\text{sat}}}{K_i k_G} s^3 + \frac{J_{\text{sat}}}{\tau_f K_i k_G} s^2 + \frac{K_P}{K_i} s + 1 \right) \tag{24}$$

The influence of external disturbance torques on the satellite's attitude is given by

$$\frac{\theta_{\text{sat}}}{T_D} = \frac{1 + \tau_f s}{\tau_f J_{\text{sat}} s^3 + J_{\text{sat}} s^2 + \tau_f K_P k_G s + \tau_f K_i k_G} \tag{25}$$

With these equations, the CATCS attitude architecture is established and is amenable to the numerical treatment in the next section.

CATCS: Attitude Actuator Performance

First, a reference mission is chosen to facilitate the numerical evaluation. The mission requirements are given in Table 1. Then, K_i is estimated according to Eq. (25) for a steady-state attitude response. Subsequently, K_P is selected as well by evaluating Eq. (24) for a closed-loop attitude stability of CATCS.

Eventually, numerical simulations (MATLAB®–Simulink™)[16] are carried out to test the developed attitude control architecture (Fig. 7). The selected gains for the simulations are $K_P = 0.8$ N · m/rad and $K_i = 0.011$ N · m/s, and k_G is regarded as unity so that the desired and exerted torque commands are directly proportional. The satellite's pitch axis moment of inertia is estimated to be $J_{\text{sat}} = 16.9$ kg · m^2. The system response time τ_f is set to 2 s, and the motors' delay, for example, 50 ms, is also considered in the simulation. The satellite reference attitude is set to $\theta_{\text{ref}} = 0$ deg.

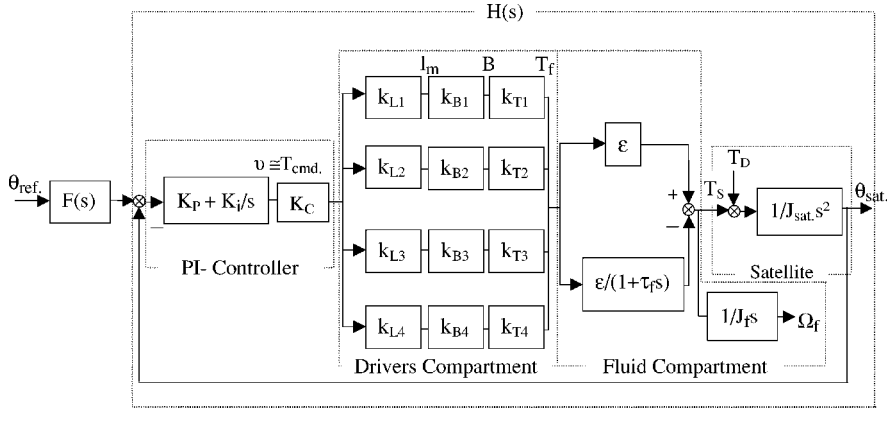

Fig. 7 CATCS attitude control architecture.

Table 1 Reference mission requirements

Requirement	Value
Mission duration	5 years
Circular orbit	500 km with inclination of 53 deg
Orbital period	95 min
Satellite mass	100 kg for a volume of $1 \times 1 \times 1$ m^3
Attitude accuracy ($\theta_{\text{sat}} - \theta_{\text{ref}}$)	Pitch $Y < 0.2$ deg
External disturbance torque $T_{D \cdot \text{pitch}}$	3.34×10^{-5} N · m $+ 2.81 \times 10^{-5}$ (sin $\Omega_o t$) N · m

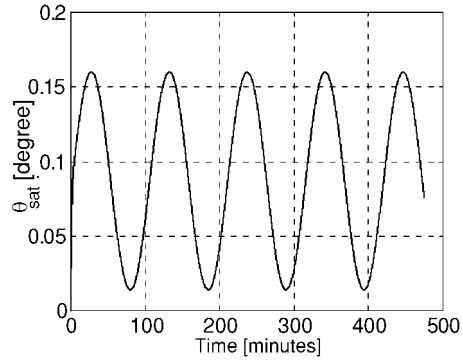

a)

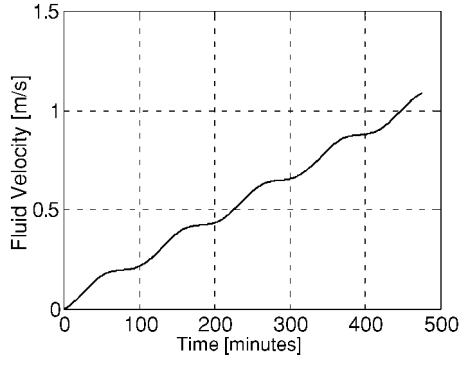

b)

Fig. 8 Ideal CATCS performance.

For the simulation, the total disturbance torque in Table 1 that is due to aerodynamics, Earth magnetic field, gravity gradient, and solar pressure is considered, which is estimated for the 100-kg cubic satellite with body-mounted solar panels.

The first test case was for an ideal CATCS, where the internal gain errors ε_T are neglected. The results are shown in Figs. 8a and 8b. In Fig. 8a the satellite's attitude is within the pointing budget ($\theta_{\text{sat}} < 0.2$ deg). On the other hand, the fluid velocity in Fig. 8b constantly increases but remains in the nominal operating range for about five orbits. Eventually, the standard available actuators, for example, gas jets or magnetic coils,[10] can be employed to reset the CATCS fluid velocity. However, the magnetic coils represent the only practical method to reset the fluid velocity without expelling propellant onboard, especially for LEO medium-class satellites. Likewise, the slew maneuver commanding procedure of reaction wheels[10] can also be adapted for CATCS if large-angle maneuvers are required without using additional actuators.

In this analysis, a nonideal case was also tested for the CATCS performance. Basically, the attitude control system in Fig. 7 will be constantly altering the magnetic flux density to keep the satellite's attitude within its pointing budget. Therefore, note that the performance of CATCS depends highly on the drivers' performances. Thus, the drivers' nonlinearities are regarded as the internal source of gain errors. These errors or disturbances would result in onboard torque errors, and their impact must be analyzed.

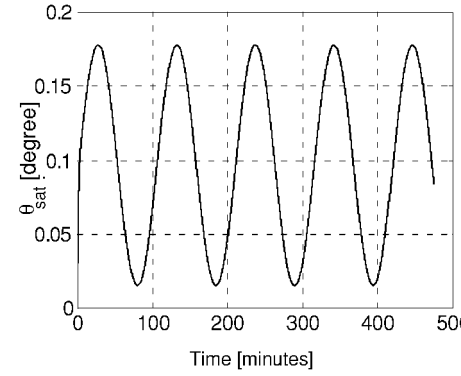

a)

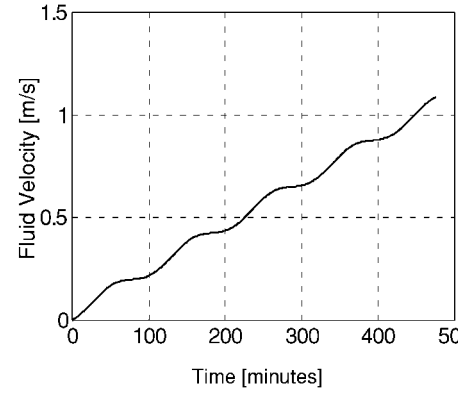

b)

Fig. 9 Nonideal CATCS performance.

The most obvious torque gain error is from the motor constants' differences, about 4% allowance[13] is given. The second internal source of disturbance is from the magnetic flux density. Because the flux is a vector field, and the condition surrounding the field would not be perfectly constant, there is always a gradient in the field due to the temperature gradient. For example, the temperature dependency of the magnetic flux density for $Nd_2Fe_{14}B$ magnets is about 0.15%/°C (Ref. 17). On the other hand, the temperature environment or margin for the onboard compartment (inner vacuum) is assumed to about 10°C (Ref. 18). Thus, the worse condition could lead to 1.5% of difference between desired and achieved magnetic flux densities. Eventually, this would induce 1.5% difference in the resulting control torque. Another source of disturbance is the temperature instability in the MHD compartments. About ±2 K is given[19] with respect to the system's temperature gradient of 50 K. This would account for 4% of difference in the generated thermoelectricity and is proportional to the system's torque gain error. Hence, macroscopically, the total system torque gain errors ε_T would account for about 9%. For this nonideal test case, all of the system gains were retained as in the preceding simulation. Despite the gain errors, the results pertaining to nonideal analysis show that the satellite attitude accuracy and fluid velocity are still within their nominal limits; see Figs. 9a and 9b, respectively. However, if desired, the attitude accuracy can be improved by increasing the K_i value accordingly.

Actually, the CATCS presented in this study can be employed for satellites up to 500 kg by using only the permanent magnets with higher magnetic flux densities, for example, up to 2 T, so that higher angular momentums, for example, up to 4 N · ms, can be achieved for the attitude control. Consequently, the CATCS heat transport capability will be also enhanced because of a higher mass transport rate in the system. On the other hand, the CATCS dimension together with the magnetic flux density must be increased accordingly for heavier satellites, for example, 1000 kg, to achieve even higher angular momentums, for example, 10–15 N · ms, to cope with their external disturbance torques, which are typically in the order of 10^{-3} N · m (Ref. 14). The results obtained and discussed up to

now focused only on the attitude control aspects. Finally, the potential benefits when compared to the existing active thermal control systems should be also taken into account. Thus, the heat transfer capability together with the mass budget of CATCS will be analyzed in the following section.

CATCS and Conventional System Comparison

The heat transfer between the duct and circulating gallium can be estimated using the heat transfer coefficient α. This coefficient is obtained from the Nusselt number Nu:

$$Nu = \alpha D/\lambda \tag{26}$$

The Nusselt number itself is a function of the Peclet number Pe:

$$Pe = V D/\kappa \tag{27}$$

As an example, the Peclet number for the thermoelectric-pump-driven CATCS ranges between 21.6 and 216.5, corresponding to medium velocities $0.05 \leq V \leq 0.5$ m/s. Thus, for $30 \leq Pe \leq 300$, the following relation[20] can be used:

$$Nu = 4.36 + 0.016\,Pe \tag{28}$$

These equations are solved for the heat transfer coefficient. Eventually, the coefficient range is $24{,}000 \leq \alpha \leq 40{,}000$ W/m$^2 \cdot$K. With the estimated heat transfer coefficient and a temperature gradient of approximately 1 K (hot and cold satellite walls), the system could transport about 400 W of heat from an area of 0.01 m^2. Also if a temperature gradient of 5 K is considered together with the estimated mass flow (0.3 kg/s), about 560 W of heat can be transported through the duct. Thus, the CATCS heat transport capability is judiciously good.

Because the CATCS is intended to substitute the conventional subsystems, the comparison is also macroscopically done considering their mass and volume budgets at the equipment level. The comparison is made with the heat pipe and reaction wheel corresponding to the total heat transport and angular momentum capabilities of CATCS, respectively. For the thermoelectric option, the total mass of gallium would be 1.9 kg. If the housing and drivers (four units all together) are also considered, then the total system mass could reach up to 2.5 kg.

Heat pipes have a good heat transport ability as well; however, in some cases (larger diameters), the mass of heat pipes appears to be critical to the overall mass budget of spacecraft. The mass of a single heat pipe can reach up to 1 kg or more depending on the type for about 500 W of heat transport.[21] On the other hand, typical reaction wheels (0.4–1.6 N$\cdot$ms) for 100–200-kg satellites have a mass budget ranging from 1.7 to 2.4 kg (Ref. 8). If a 0.4-N$\cdot$ms reaction wheel is selected for the comparison, its mass budget is about 1.7 kg. Therefore, the total mass of conventional systems (heat pipe and reaction wheel) is about 2.7 kg. Hence, the CATCS has a small mass saving (0.2 kg) here. Additionally, the effect of synergisms could also lead to indirect mass savings.[22] For example, the thermoelectric-driven CATCS requires only a very small amount of electrical power so that the performance requirements of the solar panels and batteries could be reduced in terms of their masses, especially for medium-class satellites. On the other hand, note that if the 0.4-N$\cdot$ms reaction wheel is used for the reference mission in Table 1, the wheel will be saturated within three orbital periods. Also if a higher saturation period is desired, the price in terms of mass has to be paid to have higher angular momentums onboard, which will result into a heavier reaction wheel. Likewise, the need of an electrical pump for the heat pipe system will result into higher mass, volume, and power demands onboard, which are undesirable as well.

Looking at the system volumes, the reaction wheel[8] (0.4 N$\cdot$ms) would account for a volume of 1703 cm^3, and a comparable heat pipe[21] (e.g., 3-m length, 12-mm diam, and 500 W of heat transport) with CATCS would need about 350 cm^3 of volume. Instead, the CATCS requires approximately 400 cm^3 of volume onboard. Hence, the onboard volume needed for the reaction wheel could be practically saved by employing the CATCS. In brief, the CATCS needs only the volume that is required by the heat pipe. Hence, the CATCS outperforms the uncoupled conventional systems (reaction wheel and heat pipe) from the system volume point of view. Note that the mass and volume budgets presented here would be a reasonable approximation for medium-class satellites (100–500 kg).

Discussion

In this investigation, the capability of permanent magnets is actually degraded to have a performance buffer. Note that the magnetic flux density of permanent magnets considered here is only half of the theoretical value. For example, the $Nd_2Fe_{14}B$ magnets weighing about 100 g could achieve a flux density of about 1 T for the given MHD compartment.[17] Therefore, taking into account the theoretical value, the number of pumps can be reduced to only two units for similar performance. Consequently, the reliability of CATCS would increase with lower number of pumps or drivers used, for example, magnets and linear motors. Also, because of this the total system power and mass budgets would reduce accordingly. On the other hand, if the number of pumps is maintained ($n = 4$), then the remaining CATCS momentum capacity can be used for large-angle maneuvers.

It is clear that the performance of CATCS depends also on the available onboard temperature gradient. During the safe mode (anomaly), some equipment might be switched off for reconfiguration purposes. This operation may induce lower temperature gradients in CATCS. In this case, electrical heaters could be employed to maintain the desired temperature gradient, particularly in the MHD compartments. These heaters are extremely lightweight and consume about 1 W corresponding to the temperature perheated mass, for example, 15°C/kg can be achieved in half an hour for cobalt.[23] Additionally, the heaters can be used to avoid any large temperature variations in the MHD compartments in nominal mode. Thus, the CATCS's attitude control task will always remain active, and its performance would not be hindered even in the safe mode. Moreover, during begin-of-life, these heaters can be used to partially dump the excess solar power, which is conventionally dissipated into the space environment. This benefit could actually boost the CATCS performance in terms of thermoelectric generation and result in longer operation or saturation periods, for example, >5 orbits. In addition to that, the use of better thermoelectric materials/generators could be envisaged as well for higher CATCS performance, for example, bismuth instead of cobalt. This approach also could be a solution for the CATCS to maintain its nominal performance in spacecraft with low onboard temperature gradients.

Conclusions

The concept of MHD-based CATCS has been demonstrated. The thermoelectric-driven CATCS, which benefits from the unwanted onboard temperature gradient for its operation, can be used simultaneously for the attitude and thermal control tasks. The CATCS attitude and heat transfer performances are reasonably good. All of the CATCS models presented in this study are within the mass and dimension budgets of typical satellites weighing from 100 up to 500 kg. The synergistic effects of CATCS could lead to a higher overall performance, that is, reasonable volume savings, heat transport enhancement, or even small mass/power savings for a certain satellite mission. A CATCS prototype design accounting for the spacecraft compartment will allow the characterisation of system gains, especially for the MHD drivers. Finally, this investigation offers a feasible synergism for future medium-class spacecraft.

Acknowledgments

Financial support for R. Varatharajoo from the Malaysian Government is gratefully acknowledged. The authors thank G. Gerbeth at Rossendorf Research Center and J. Stiller and T. Roschke at Dresden University of Technology for useful discussions. The consultations with C. M. Roithmayr and T. Michalis at NASA and R. Moreau at the Centre National de la Recherche Scientifique are also appreciated.

References

[1]Varatharajoo, R., and Fasoulas, S., "Synergisms for Spacecraft Attitude Control System," *Proceedings of World Space Congress*, International Astronautics Federation, Paris, 2002, pp. 1–11.

[2]Fasoulas, S., Varatharajoo, R., and Kahle, R., "Raumfahrzeug mit einer Einrichtung zur Wärmeregelung," German Patent Pending 10230349.5, Munich, June 2002, pp. 1–33.

[3]Fasoulas, S., Varatharajoo, R., and Kahle, R., "Raumfahrzeug mit einer Einrichtung zur Lageregelung," German Patent Pending 10230350.9, Munich, June 2002, pp. 1–38.

[4]Douglas, J. F., Gasiorek, J. M., and Swaffield, J. A, *Fluid Mechanics*, 2nd ed., Longman, Harlow, 1985, pp. 244–246.

[5]Heinrich, G., *Einführung in die konvektive Wärme-und Stoffübertragung*, 1st ed., Verlag Technik, Berlin, 1990, pp. 156–157.

[6]Idelchik, I. E., *Handbook of Hydraulic Resistance*, 3rd ed., Begell House, New York, 1994, pp. 361, 362.

[7]Moreau, R., *Magnetohydroynamics*, 1st ed., Kluwer, Dordrecht, The Netherlands, 1990, pp. 17, 124–126.

[8]"Momentum and Reaction Wheels," Teldix GmbH, Rept. RSI 04-25/60, Heidelberg, Germany, June 2000, pp. 1–2.

[9]Shercliff, J. A., "Thermoelectric Magnetohydrodynamics," *Journal of Fluid Mechanics*, Vol. 91, May 1979, pp. 231–251.

[10]Wertz, J. R. (ed.), *Spacecraft Attitude Determination and Control*, 7th ed., Kluwer, Dordrecht, The Netherlands, 1994, pp. 202, 566–576, 602, 655–657.

[11]Messadek, K., and Moreau, R., "An Experimental Investigation of MHD Quansi-Two-Dimensional Turbulent Shear Flows," *Journal of Fluid Mechanics*, Vol. 456, April, 2002, pp. 137–159.

[12]Roschke, T., Gollee, R., and Gerlach, G., "Dynamic Analysis of Electromagnetic Actuators," *Proceedings of Workshop on System Design Automation SDA' 98*, German Collaborative Research Center, Dresden, Germany, 1998, pp. 135–143.

[13]Favre, E., "European Handbook—Electric Motors for Space Applications," ESA, Rept. ESMH.401, No. 4, Noordwijk, The Netherlands, Jan. 2001, pp. 68, 69, 156.

[14]Sidi, M., *Spacecraft Dynamics and Control, A Practical Engineering Approach*, 1st ed., Cambridge Univ. Press, New York, 1997, pp. 129, 193, 241, 242.

[15]Varatharajoo, R., and Fasoulas, S., "Methodology for the Development of Combined Energy and Attitude Control Systems for Satellites," *Aerospace Science and Technology*, Vol. 6 , No. 4, 2002, pp. 303–311.

[16]"MATLAB: The Language of Technical Computing–Computation, Visualization and Programming," Ver. 6.0.0.88, Release 12, MathWorks, Natick, MA, Sept. 2000.

[17]"Rare-Earth Permanent Magnets," Vacuumschmelze GmbH, Rept. Vacodym/Vacomax PD-002, Hanau, Germany, March 2000, pp. 14–31.

[18]Larson, J. W., and Wertz, J. R. (eds.), *Space Mission Analysis and Design*, 2nd ed., Kluwer, Dordrecht, The Netherlands, 1997, pp. 415, 416.

[19]"Space Engineering—Mechanical—Part 1: Thermal Control," ESA, Rept. ECSS-E-30-Part 1A, Noordwijk, The Netherlands, April 2000, pp. 41, 42.

[20]Firsova, E. V., and Lebedev, M. E., *Heat Exchanger Handbook, Heat Transfer in Liquid Metals*, 1st ed., Begell House, New York, 1998, pp. 2.5.13.1–2.5.13.10.

[21]Messerschmid, E., and Fasoulas, S., *Raumfahrtsysteme*, 1st ed., Springer-Verlag, Berlin, 2000, pp. 353–355.

[22]Messerschmid, E., and Bertrand, R., *Space Stations System and Utilization*, 1st ed., Springer-Verlag, Berlin, 1999, pp. 371, 372.

[23]"Estimating Power Requirements of Thermofoil Heaters," Minco Products, Inc., Rept. AA 21-890403-1, Minneapolis, MN, Dec. 2001, pp. 1–8.

I. E. Vas
Associate Editor